AGU PUBLICATIONS

Geophysical Research Letters

RESEARCH LETTER

10.1002/2014GL062749

Key Points:
- Cloud slicing with lidar can sense CO_2 in the planetary boundary layer
- Lidar cloud slicing has been demonstrated using cumulus and cirrus clouds
- Lidar cloud slicing was validated with in situ measurements

Correspondence to:
A. K. Ramanathan,
anand.ramanathan@nasa.gov

Citation:
Ramanathan, A. K., J. Mao, J. B. Abshire, and G. R. Allan (2015), Remote sensing measurements of the CO_2 mixing ratio in the planetary boundary layer using cloud slicing with airborne lidar, *Geophys. Res. Lett.*, *42*, 2055–2062, doi:10.1002/2014GL062749.

Received 3 DEC 2014
Accepted 17 FEB 2015
Accepted article online 23 FEB 2015
Published online 27 MAR 2015

Remote sensing measurements of the CO_2 mixing ratio in the planetary boundary layer using cloud slicing with airborne lidar

Anand K. Ramanathan[1,2], Jianping Mao[1,3], James B. Abshire[2], and Graham R. Allan[2,4]

[1]Earth System Science Interdisciplinary Center, University of Maryland, College Park, Maryland, USA, [2]Solar System Exploration Division, NASA Goddard Space Flight Center, Greenbelt, MD, USA, [3]Earth Sciences Division, NASA Goddard Space Flight Center, Greenbelt, Maryland, USA, [4]Sigma Space Corporation, Lanham, Maryland, USA

Abstract We have measured the CO_2 volume mixing ratio (VMR) within the planetary boundary layer (PBL) using cloud slicing with an airborne pulsed integrated path differential absorption (IPDA) lidar from flight altitudes of up to 13 km. During a flight over Iowa in summer 2011, simultaneous measurement of the optical range and CO_2 absorption to clouds and the ground were made using time-resolved detection of pulse echoes from each scattering surface. We determined the CO_2 absorption in the PBL by differencing the two lidar-measured absorption line shapes, one to a broken shallow cumulus cloud layer located at the top of the PBL and the other to the ground. Solving for the CO_2 VMR in the PBL and that of the free troposphere, we measured a ≈15 ppm (4%) drawdown in the PBL. Both CO_2 VMRs were within ≈3 ppm of in situ CO_2 profile measurements. We have also demonstrated cloud slicing using scatter from thin, diffuse cirrus clouds and cumulus clouds, which allowed solving for the CO_2 VMR for three vertical layers. The technique and retrieval algorithm are applicable to a space-based lidar instrument as well as to lidar IPDA measurements of other trace gases. Thus, lidar cloud slicing also offers promise toward space-based remote sensing of vertical trace gas profiles in the atmosphere using a variety of clouds.

1. Introduction

Satellite remote sensing of carbon dioxide (CO_2) in the lower atmosphere is key to identifying and monitoring global CO_2 sources and sinks for improving our understanding of the global carbon cycle [*Rayner and O'Brien*, 2001]. Current satellites such as the Greenhouse Gas Observing Satellite (GOSAT) [*Kuze et al.*, 2009] and the Orbiting Carbon Observatory-2 [*Crisp et al.*, 2004; *Boesch et al.*, 2011] measure the total column absorption of CO_2 in sunlight reflected from the Earth's surface and thus respond near uniformly to CO_2 in the atmospheric column to the scattering surface. CO_2 surface fluxes make only small changes to the total column signal. In addition, CO_2 measurements can be made only over cloud-free, sunlit areas of the Earth and are susceptible to biases in the presence of aerosols or thin clouds [*Mao and Kawa*, 2004; *Guerlet et al.*, 2013]. To overcome these limitations of passive remote sensing satellites, NASA commissioned the formulation study of ASCENDS (Active Sensing of CO_2 Emissions over Nights, Days, and Seasons), a space-based lidar mission. The NASA Goddard Space Flight Center CO_2 Sounder lidar is one candidate approach for the ASCENDS mission.

The NASA Goddard CO_2 Sounder is a pulsed lidar using an integrated path differential absorption (IPDA) measurement approach [*Abshire et al.*, 2010]. The pulsed approach with a time-resolved receiver enables accurate gas absorption line shape measurements to a scattering surface even in the presence of weak scattering in the optical path. Previously, we demonstrated accurate (bias <1.3 ppm) airborne lidar measurements of the total column-averaged CO_2 volume mixing ratio (VMR) [*Abshire et al.*, 2014]. In this work, we take advantage of the range and gas absorption information in time-resolved cloud backscatter and demonstrate CO_2 VMR measurements in the planetary boundary layer (PBL) using cloud slicing. Such measurements are more responsive to CO_2 surface fluxes than are total column measurements.

Cloud slicing, a technique first applied to differential optical absorption measurements from passive spectrometers [*Ziemke et al.*, 2001], divides the atmosphere into cloud-separated layers and measures the gas column absorption in each layer using optical scatter from the cloud tops. Cloud slicing has been used to measure upper tropospheric column ozone [*Ziemke et al.*, 2001] and the VMR of nitrogen dioxide [*Choi et al.*,

©2015. American Geophysical Union. All Rights Reserved.

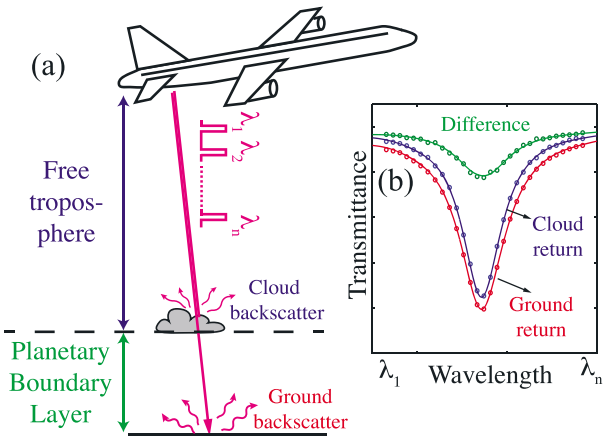

Figure 1. Schematic showing lidar cloud slicing with a thin, shallow planetary boundary layer (PBL) cloud: (a) The CO_2 IPDA lidar measures the two-way atmospheric transmittance to each scattering surface in the light path. (b) From these, one can determine the transmittance of each cloud-separated layer of the atmosphere (here the PBL and the free troposphere) and retrieve the corresponding CO_2 volume mixing ratios.

2014] and carbon monoxide [*Liu et al.*, 2014] in the troposphere. A ground-based lidar [*Gibert et al.*, 2008] has also used clouds as a scattering target to measure the CO_2 mixing ratio in the PBL.

The concept of cloud slicing using an airborne lidar is illustrated in Figure 1. When the plane flies over a layer of thin or broken clouds (Figure 1a), the IPDA lidar measures the two-way wavelength-resolved atmospheric transmittance to each scattering surface (Figure 1b). From these, one can determine the gas-transmittance line shape of each cloud-separated layer of the atmosphere. One can then retrieve the precise column-averaged VMR of the gas for each atmospheric layer using radiative transfer modeling of the gas absorption. We take advantage of the fact that cumulus clouds often occur at the top of the PBL [*Stull*, 1988] and, using a layer of shallow (compared to PBL height) cumulus clouds, demonstrate lidar cloud slicing to measure the CO_2 VMR within the PBL.

2. Instrument Description and Methods

2.1. The CO_2 Sounder Instrument

The CO_2 Sounder lidar instrument was flown on the NASA DC-8 during the NASA ASCENDS campaign in 2011 at altitudes of up to 13 km above sea level, below which ≈80% of the atmosphere by mass resides. The laser transmitted a train of 1 μs wide square pulses with ≈22 μJ energy per pulse at a 10 kHz rate. The source laser wavelength was scanned linearly every ≈3 ms in a repeating sawtooth pattern, which allowed the transmitted pulses to sample the 1572.335 nm CO_2 absorption line (30012 ← 00001 R16e) with 30 wavelengths. This allowed a high-resolution measurement of the absorption line shape and better correction for Doppler shifts and the system wavelength response. In fitting the absorption line shape, the loss in signal-to-noise ratio for individual wavelength samples is compensated by the larger number of wavelength samples. In flight, we calibrated the wavelength scan using optical heterodyne detection with a second, wavemeter-referenced laser. During operation, the transmitted wavelengths stayed constant, except for a <0.4 pm/h, slowly varying overall wavelength offset, which was monitored and corrected for in postflight analysis. The outgoing energy of individual pulses was recorded to allow for normalizing energy variations in the transmitted pulses.

The transmitted lidar beam was directed toward nadir from the aircraft. The lidar receiver used a 20 cm diameter telescope to collect the backscatter, and a high-gain infrared photomultiplier tube (PMT) followed by a discriminator as a photon counting detector. These photon counts binned by their arrival time relative to the start of the wavelength scan and synchronously accumulated over ≈300 wavelength scans (≈900 ms) before the data were transferred to the lidar's computer. The lidar recorded data in 1 s intervals. The full system parameters are listed in *Abshire et al.* [2014].

The receiver PMT-discriminator response to light intensity deviated from linear with increasing photon count rate. For typical lidar return intensities, the deviation was around 5%. The nonlinear response was calibrated in the laboratory prior to the field campaign. This calibration was refined using airborne

 ©2015. American Geophysical Union. All Rights Reserved.

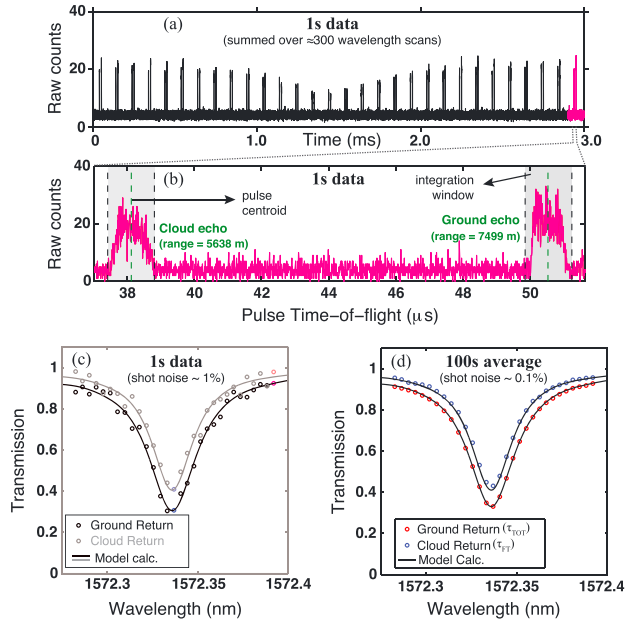

Figure 2. (a) A sample of lidar backscatter versus time for 1 s accumulated data with both cloud and ground returns showing the CO_2 absorption shape: Each pair of vertical lines correspond to the time-resolved cloud and ground echoes for the 30 wavelengths probed. (b) Expanded time base for a single wavelength showing fully time-resolved backscatter. (c) Wavelength samples (circles) of the transmittance line shapes from integrating individual pulses from each set of 30 pulse echoes. (d) Wavelength samples averaged for 100 s to reduce photon shot noise.

measurements of a well-characterized atmosphere that were made over Railroad Valley, Nevada, USA, on 3 August 2011 during the campaign. The calibration method is similar to that of calibrating satellite instruments such as GOSAT [*Kuze et al.*, 2011]. No bias correction was used during the retrieval process.

2.2. CO_2 Mixing Ratio Retrievals

In postflight analysis, the measured transmittance line shape and optical range were extracted from the 1 s accumulated lidar backscatter data (Figure 2a). Pulse echo signals from the cloud and ground were separated by time of flight (Figure 2b). Based on the photon count statistics, the noise visible in the pulse echoes can be attributed to photon shot noise. Under ideal conditions, when flying level over a flat surface, the optical range computed from the pulse time of flight has ~1 m precision [*Abshire et al.*, 2014]. Since the echo pulses can be broadened by diffuse scattering surfaces (clouds) or by aircraft tilt, the retrieval algorithm computes the range using the pulse centroid. The optical range, combined with the aircraft Global Positioning System altitude and pitch and roll information gives the vector optical path of the lidar pulses, which was used for modeling the transmittance (Figure 2c) and retrieving the CO_2 VMR.

To determine the atmospheric transmittance line shape, the algorithm first integrates the lidar pulses (Figure 2b) and subtracts the solar background and factors in the wavelength calibration, thereby obtaining the return pulse energies $E(\lambda_i)$ in units of integrated photon counts. The algorithm then normalizes $E(\lambda_i)$ by the outgoing energy $E_0(\lambda_i)$ and the off-line pulse energy (all energies are accumulated over the 1 s interval) to get the transmittance line shape (Figure 2c):

$$\tau(\lambda_i) = \tau_{\text{off}} \times \frac{E(\lambda_i)/E_0(\lambda_i)}{\langle E(\lambda_{\text{off}})/E_0(\lambda_{\text{off}})\rangle}, \quad \lambda_{\text{off}} \in \{\lambda_2 \ldots \lambda_5, \lambda_{26} \ldots \lambda_{30}\} \tag{1}$$

where τ_{off} sets the appropriate scale and $\langle E(\lambda_{\text{off}})/E_0(\lambda_{\text{off}})\rangle$ is the off-line return pulse energy averaged over all off-line wavelengths.

For a cloud layer at the top of the PBL (Figure 1a) with the cloud thickness being small compared to the PBL column, the cloud divides the atmosphere into two layers, the PBL and free troposphere (FT). The line shape measured from the cloud return $E_{\text{cl}}(\lambda_i)$ yields the transmittance of the FT, $\tau_{\text{FT}}(\lambda_i)$, while the line shape from the ground return $E_{\text{gr}}(\lambda_i)$ yields the total column transmittance, $\tau_{\text{TOT}}(\lambda_i)$, which can be expressed as

$$\tau_{\text{TOT}}(\lambda_i) = \tau_{\text{FT}}(\lambda_i) \times \tau_{\text{PBL}}(\lambda_i), \tag{2}$$

©2015. American Geophysical Union. All Rights Reserved.

where $\tau_{PBL}(\lambda_i)$ is the PBL transmittance. Equation (2) can also be expressed in terms of optical depth, $OD = -\ln \tau$ so that $OD_{TOT}(\lambda_i) = OD_{FT}(\lambda_i) + OD_{PBL}(\lambda_i)$. The OD or absorption line shape better resolves line shape properties such as pressure broadening [*Ramanathan et al.*, 2013].

To retrieve the CO_2 VMR from the transmittance $\tau(\lambda_i)$, the algorithm uses a radiative transfer model based on the *Clough et al.* [2005] line-by-line radiative transfer model and HITRAN (High Resolution Transmission) 2008 [*Rothman et al.*, 2009]. Corresponding to each measurement $\tau(\lambda_i)$, the model calculates $\tau_{model}(\lambda)$ using the cloud (or ground) elevation from the optical range and the atmospheric pressure, temperature, and water vapor profile from the Modern Era Retrospective Analysis For Research and Applications (MERRA, compiled by the NASA Global Modeling and Assimilation Office) model. The algorithm uses no a priori CO_2 information and fits for a uniform CO_2 distribution and a single CO_2 VMR parameter, X_{CO_2} representing the entire column. After two minor adjustments to $\tau(\lambda_i)$, fitting and correcting for a small wavelength offset (<0.2 pm), and a small, linear baseline system wavelength response, the algorithm minimizes,

$$\chi^2(X_{CO_2}) = \sum_{\lambda_{on}} W(\lambda_i)\left(1 - \frac{\tau(\lambda_i)}{\tau_{model}(\lambda_i, X_{CO_2})}\right)^2, \quad \lambda_{on} \in \{\lambda_6 \ldots \lambda_{25}\} \tag{3}$$

as a function of X_{CO_2}. $W(\lambda_i)$ is a weighting function to factor in the heterogeneity of the wavelength samples (discussed below). The retrieval algorithm thus described was used in [*Abshire et al.*, 2014].

For the results shown in this letter, we averaged the data over a ≈20 km ground track (100 s in time), both to reduce photon shot noise (see Figure 2d) and to allow sufficient backscatter from both the cloud and ground reflecting surfaces. Within each 100 s interval, there was a mixture of 1 s data with returns from cloud only, ground-only and simultaneous cloud and ground (example shown in Figures 2a–2c). Our algorithm accommodates averaging varying numbers of cloud and ground echoes.

The steps in the retrieval were as follows: First, for every 1 s of data with a cloud or ground return, we calculated the model transmittance for each return using the vector optical path and radiative transfer modeling. Then, we summed individual 1 s data, $E_{cl}(\lambda_i)$ and $E_{gr}(\lambda_i)$ for each 100 s time interval. Next, we correspondingly averaged the 1 s radiative transfer model calculations over the same interval to obtain the model transmittances $\tau_{FT,model}(\lambda)$ and $\tau_{TOT,model}(\lambda)$, respectively. Then, we normalized the summed lidar return energies using equation (1) with $\tau_{off} = \langle \tau_{model}(\lambda_{off}) \rangle$ and computed the measured transmittances $\tau_{FT}(\lambda_i)$ and $\tau_{TOT}(\lambda_i)$ (Figure 2d). We then computed the PBL-measured and model transmittances $\tau_{PBL}(\lambda_i)$ and $\tau_{PBL,model}(\lambda)$ using equation (2). Finally, we retrieved the CO_2 VMR in the FT and the PBL by performing individual minimizations of equation (3) for each layer.

For the FT retrieval, we used a weighting function

$$W_{FT}(\lambda_i) = \frac{OD_{FT}(\lambda_i)E_{cl}(\lambda_i)}{\sqrt{E_{cl}(\lambda_i)}} \tag{4}$$

that factors in the sensitivity ($OD(\lambda_i)E(\lambda_i)$) of each wavelength λ_i to a change in X_{CO_2} and the photon shot noise ($\sqrt{E(\lambda_i)}$) associated with the wavelength sample. In our experience, this weighting function works the best across a range of flight altitudes and signal levels [*Abshire et al.*, 2014]. For the PBL, we used an analogous weighting function

$$W_{PBL}(\lambda_i) \approx \frac{E_{gr}(\lambda_i)E_{cl}(\lambda_i)OD_{PBL}(\lambda_i)}{\sqrt{E_{gr}(\lambda_i)E_{cl}^2(\lambda_i) + E_{gr}^2(\lambda_i)E_{cl}(\lambda_i)}} \tag{5}$$

to weight the least squares fit. After fitting, we characterized the quality of each retrieval by the signal-to-noise ratio of the retrieved CO_2 VMR, SNR_X estimated by propagating photon shot noise in E_{gr} and E_{cl} through the steps of the retrieval. We did not include the solar background on the detector in the SNR_X estimates as it was found to be relatively low (see Figures 2a and 2b) and had little impact on the overall signal-to-noise ratio.

2.3. Flight Over Iowa on 10 August 2011

In the ASCENDS flight over Iowa on 10 August 2011 (Figure 3a), there were fair weather broken shallow cumulus clouds (Figure 3a). The aircraft flew over the same ground track at altitudes ranging from 3 to 13 km followed by a descent spiral from 13 km to the ground over the center of the track. Lidar backscatter revealed a flat terrain (range of elevations 180–300 m above mean sea level) and shallow, level cumulus

©2015. American Geophysical Union. All Rights Reserved.

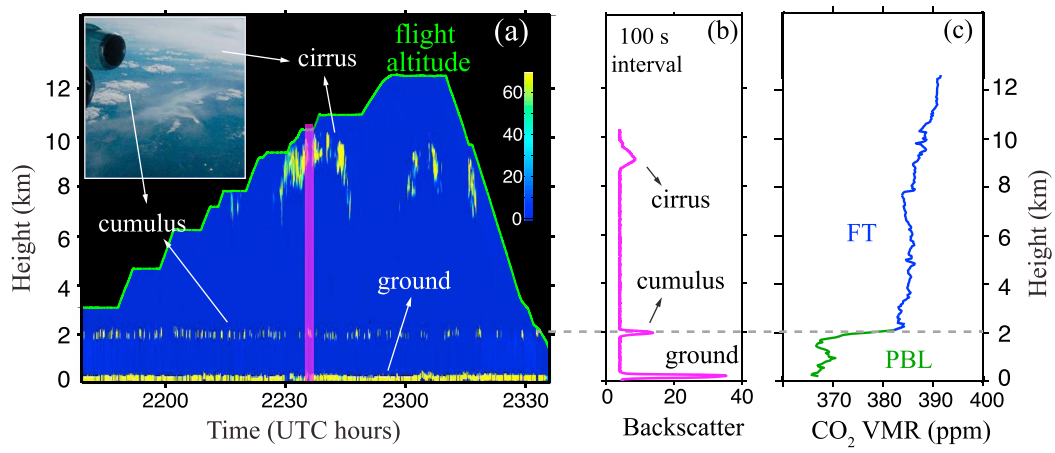

Figure 3. Flight conditions over Iowa on 10 August 2011. (a) Lidar backscatter profile measured for the flight segment show returns from the ground, cumulus clouds and cirrus clouds. Inset: photograph taken from the airplane. (b) A sample backscatter profile for a 100 s interval beginning at 2235 UTC (magenta rectangle in Figure 3a). (c) The CO_2 vertical profile measured from the aircraft using an on-board in situ CO_2 sensor shows a sharp ≈15 ppm decrease in the CO_2 VMR in the PBL, just below the cumulus clouds.

clouds (range of cloud top elevations 1950–2200 m) at the PBL. These conditions provided an excellent opportunity to perform cloud slicing, by allowing averaging over the ≈20 km ground track (100 s in time) with little change in elevation. In addition, measurements from an on-board in situ CO_2 sensor (described in *Vay et al.* [2003]) that continuously monitored the CO_2 VMR in the air outside the aircraft showed a strong, ≈15 ppm VMR reduction in the PBL due to photosynthesis in the growing summer crop (predominantly corn) in Iowa (Figure 3c). The VMR reduction has also been seen in total column lidar measurements from the flight [*Menzies et al.*, 2014; *Abshire et al.*, 2014]. The ≈1 ppm (in the FT) and ≈2–5 ppm (in the PBL) along-track variation of the CO_2 VMR were smaller than the vertical PBL-FT difference.

3. Results

3.1. Two-Layer Cloud Slicing Using Cumulus Clouds

The measured CO_2 absorption line shapes (see Figure 4a) of the total column and FT averaged over the 100 s interval were found to fit well with model calculations enabling two-layer cloud slicing

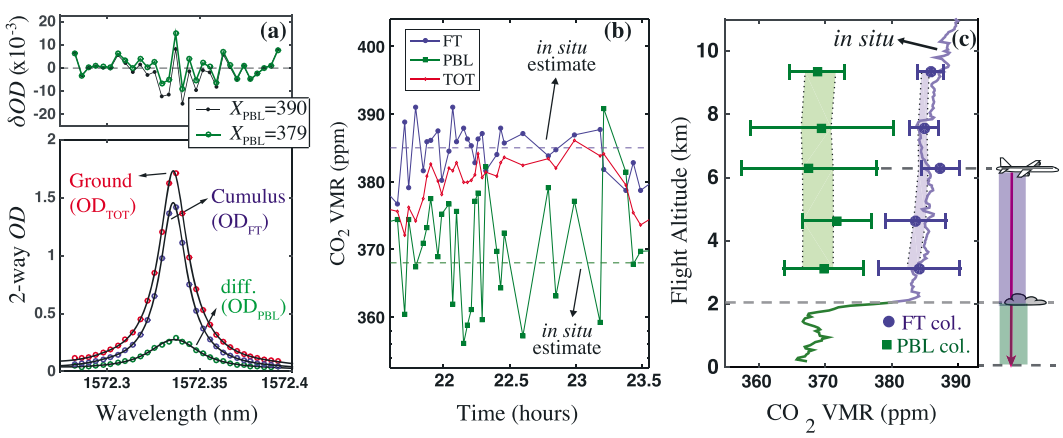

Figure 4. Cloud slicing CO_2 measurements over Iowa on 10 August 2011. (a) Sample measured absorption line shapes (flight altitude ≈11 km) and residuals ((top) data-model) of the PBL line shape. For this retrieval, $X_{CO_2,PBL}$ = 379 ppm (SNR_X = 85) was found to be optimum. (b) For the flight segment shown in Figure 3a, PBL retrievals (green squares), in contrast to total column retrievals (red diamonds) showed a clear ≈15 ppm CO_2 drop relative to FT retrievals (blue circles). (c) Lidar CO_2 VMR measurements were aggregated to obtain the mean (solid points) and standard deviation (error bars) for each flight altitude, which agreed well with calculated in situ column measurements (shaded regions) derived from the in situ CO_2 profile (solid line). The shaded areas reflect the along-track variability of the atmospheric CO_2 VMR. A summary of the data is also shown in Table 1.

©2015. American Geophysical Union. All Rights Reserved.

Table 1. Summary of Two-Layer Cloud Slicing Results Over Iowa on 10 August 2011—Lidar Cloud Slicing Retrievals Aggregated by Flight Altitude Were Validated by In Situ Measurements Averaged Over the Lidar Column[a]

		Planetary Boundary Layer (PBL)					Free Troposphere (FT)				
Altitude (km)	Samples	In Situ Ref. (ppm)	Lidar Mean (ppm)	SNR_X Average	Lidar SD (ppm)	Bias (ppm)	In Situ Ref. (ppm)	Lidar Mean (ppm)	SNR_X Average	Lidar SD (ppm)	Bias (ppm)
3.11	5	368.9	369.8	125	6.0	0.9	383.2	384.1	80	6.1	1.0
4.64	11	368.9	371.8	95	5.2	2.9	384.2	383.6	140	4.6	−0.6
6.29	4	368.9	367.6	90	10.2	−1.3	384.8	387.3	220	2.8	2.6
7.58	6	368.6	369.5	75	10.8	0.9	384.6	384.9	230	2.2	0.3
9.36	3	369.3	368.8	65	4.1	−0.5	385.1	385.9	245	2.0	0.8

[a]The bias in the lidar retrievals (lidar-in situ), measured at five distinct altitudes was small, limited primarily by sample size.

measurements of the CO_2 VMR. For the sample plot and residual shown in Figure 4a, the PBL fit residuals showed a clear improvement with the RMS residual decreasing from 5.8×10^{-3} (units of OD) to 5.0×10^{-3} when the model $X_{CO_2,PBL}$ was lowered from 390 ppm to 379 ppm. After performing cloud slicing retrievals for the entire flight segment shown in Figure 3, we applied the following data-screening process: ≈45% of the 100 s interval data were rejected because of poor measurement significance (criterion: $SNR_X < 50$) arising from weak cloud or ground echoes. Additionally, ≈5% of data were rejected for poor modeling of atmospheric absorption (excess noise ratio [*Abshire et al.*, 2014], >1.5) and ≈1% for poor vertical colocation of cloud and ground returns (change in flight altitude>300 m); ≈50% of the total data passed the screening process. The column-averaged PBL and FT CO_2 VMRs are plotted in Figure 4b.

We assessed the accuracy of lidar cloud slicing CO_2 VMR measurements by comparing them to the in situ CO_2 profile. First we aggregated lidar data to obtain the mean and standard deviation of the CO_2 VMRs at each flight altitude (Figure 4c). Then, we calculated the column-averaged in situ CO_2 VMR for the PBL and the FT to compare against the lidar data (see Table 1). The lidar measurements were found to be in good agreement with in situ data at all five flight altitudes for which we had a sufficient sample size (≥3) of 100 s averaged data points.

The cloud slicing PBL measurements had a lower SNR_X compared to the FT measurements (Table 1). This is because, in cloud slicing, photon shot noise from both cloud and ground returns is projected onto a smaller absorption signal (OD, see Figure 4a), resulting in a lower SNR_X. This lower SNR_X and the higher variability of the PBL CO_2 caused PBL CO_2 VMR measurements to have larger scatter ($1\sigma \approx 10$ ppm) compared to those of the FT (2 ppm).

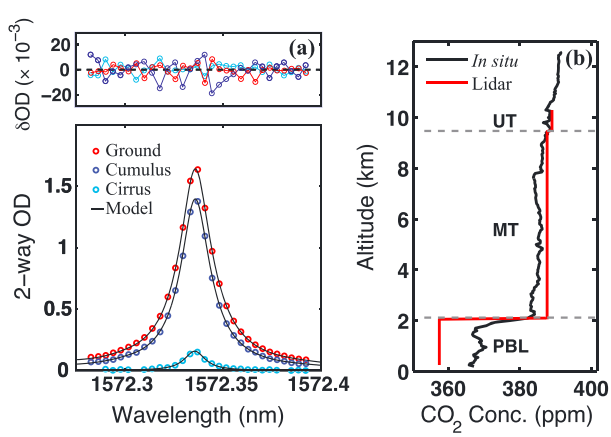

Figure 5. Three-layer cloud slicing using cirrus and cumulus clouds: (a) Line shapes from cirrus, cumulus, and ground backscatter for the 100 s interval plotted in Figure 3b. The low fit residuals (top, data-model) show that the absorption in the atmospheric layers is in good agreement with model calculations. (b) The retrieved three-layer CO_2 VMR profile is in good agreement with the in situ profile, limited by the signal-to-noise ratio.

©2015. American Geophysical Union. All Rights Reserved.

3.2. Three-Layer Cloud Slicing Using Cumulus and Cirrus Clouds

We have also demonstrated cloud slicing using backscatter from upper level cirrus clouds and lower level cumulus clouds. For the 100 s segment beginning at 2235 UTC shown in Figure 3b, additional backscatter from a cirrus cloud layer at around 9 km was strong enough to measure the absorption (Figure 5a). Since the cirrus cloud depth was nearly 1.5 km, we used only the backscatter from the top 500 m to keep the reflecting layer thin compared to the atmospheric column. Thus, we split the FT into two layers corresponding to the upper troposphere (plane-cirrus) and midtroposphere (cirrus-cumulus), which, along with the PBL, made three layers in all.

The upper troposphere, midtroposphere, and PBL CO_2 VMRs measured using cloud slicing were 389 ppm ($SNR_X = 45$), 387 ppm (295), and 357 ppm (85), respectively (Figure 5b). The measured three-layer CO_2 profile, factoring in the limited SNR, was in good agreement with in situ data. In addition, model calculations fit the measured absorption line shapes well (residuals plotted in Figure 5a). The limited number of three-layer measurements with sufficient SNR prevented us from generating aggregated statistics.

4. Discussion

The retrieved CO_2 VMRs using cloud slicing were photon shot noise limited with no evidence of bias. Standard deviations in the aggregated CO_2 VMRs were in agreement with the corresponding computed SNRs (see Table 1). With planned improvements to the lidar such as a more sensitive detector and the use of higher laser pulse energies, we expect more stringent tests of the technique and checks for biases in the cloud slicing retrievals.

In using cloud slicing to determine the transmittance of the atmospheric column below the cloud, no assumptions are required as long as the variation in the cloud layer elevation is small compared to the upper and lower atmospheric column heights. In addition, potential systematic effects such as the variability in the system wavelength response are common to both and cancel. Thus, in retrieving X_{CO_2} for the lower layer (PBL in this work), one needs information about the atmospheric pressure, temperature, and water vapor profile only for the lower layer, making such retrievals more robust.

Lidar cloud slicing has several advantages over similar techniques using passive instruments [*Ziemke et al.*, 1998]. The time-resolved lidar backscatter from the cloud provides a clear delineation of the cloud top and the precise boundary between the upper and lower atmospheric layers. In addition, as demonstrated, lidar cloud slicing works well with thin or broken clouds allowing for excellent colocation of absorption measurements to different scattering surfaces. Finally, the high spectral resolution of lidar measurements makes them more sensitive to the absorption line shape and consequently less prone to biases from the instrument or other factors.

5. Conclusion and Future Work

In summary, we have demonstrated cloud slicing using an airborne IPDA lidar to obtain the CO_2 VMR in the FT and the PBL and have validated the measurements using in situ data. Such PBL CO_2 VMR measurements are more responsive to CO_2 fluxes. We have also demonstrated cloud slicing using a thin cirrus cloud layer. Future work will focus on collecting more data with cirrus clouds for better statistics and enhancing the retrieval algorithm to use other cloud types such as towering cumulus and multilayer cirrus. The impact of cloud slicing retrievals on CO_2 flux retrievals will also be studied.

For a CO_2 IPDA lidar on a satellite, cloud slicing may be used with a variety of clouds. For cumulus and altocumulus clouds, which occur over ≈20% of the Earth's surface [*Sassen and Wang*, 2008], cloud slicing yields the PBL or lower tropospheric CO_2 VMR depending on cloud elevation. For cirrus clouds, which occur over more than 15% of the Earth's surface [*Sassen et al.*, 2008], cloud slicing enables making separate CO_2 VMR measurements of the stratosphere and troposphere. In addition, CO_2 profile information obtained from multilayer cloud slicing could help improve our understanding of CO_2 mixing in the midtroposphere and CO_2 transport over regional scales [*Tiwari et al.*, 2006]. This is currently being studied by the ASCENDS formulation team (S. R. Kawa, private communication, 2014).

The technique and retrieval algorithm described here are also applicable to the remote sensing of other trace gases such as CH_4. Airborne pulsed IPDA lidar measurements of CH_4 [*Riris et al.*, 2012] have been

©2015. American Geophysical Union. All Rights Reserved.

demonstrated, and work toward space-based measurements is underway [*Stephan et al.*, 2011]. Thus, with the increasing use of IPDA lidar, we expect lidar cloud slicing to play an important role in making vertically resolved measurements of trace gases.

Acknowledgments
This work was funded by the NASA ESTO IIP-10 program and the NASA ASCENDS formulation activity. A.K.R. acknowledges initial support from the NASA Postdoctoral Program. We also thank the AVOCET team of NASA LaRC for providing the in situ CO_2 VMR measurements, the NASA DAOF DC-8 team for help in conducting the flight campaign, and S. Randy Kawa for providing the MERRA data used for the analysis. We also thank the anonymous reviewers for their helpful comments and suggestions. Data available on request.

The Editor thanks two anonymous reviewers for their assistance in evaluating this paper.

References

Abshire, J. B., H. Riris, G. R. Allan, C. J. Weaver, J. Mao, X. Sun, W. E. Hasselbrack, S. R. Kawa, and S. Biraud (2010), Pulsed airborne lidar measurements of atmospheric CO_2 column absorption, *Tellus B*, *62*(5), 770–783.

Abshire, J. B., A. Ramanathan, H. Riris, J. Mao, G. R. Allan, W. E. Hasselbrack, C. J. Weaver, and E. V. Browell (2014), Airborne measurements of CO_2 column concentration and range using a pulsed direct-detection IPDA lidar, *Remote Sens.*, *6*(1), 443–469, doi:10.3390/rs6010443.

Boesch, H., D. Baker, B. Connor, D. Crisp, and C. Miller (2011), Global characterization of CO_2 column retrievals from shortwave-infrared satellite observations of the orbiting carbon observatory-2 mission, *Remote Sens.*, *3*(2), 270–304.

Choi, S., J. Joiner, Y. Choi, B. Duncan, and E. Bucsela (2014), Global free tropospheric no_2 abundances derived using a cloud slicing technique applied to satellite observations from the aura Ozone Monitoring Instrument (OMI), *Atmos. Chem. Phys. Discuss.*, *14*(2), 1559–1615.

Clough, S. A., M. W. Shephard, E. J. Mlawer, J. S. Delamere, M. J. Iacono, K. Cady-Pereira, S. Boukabara, and P. D. Brown (2005), Atmospheric radiative transfer modeling: A summary of the AER codes, *J. Quant. Spectros. Radiat. Transfer*, *91*(2), 233–244.

Crisp, D., et al. (2004), The Orbiting Carbon Observatory (OCO) mission, *Adv. Space Res.*, *34*(4), 700–709.

Gibert, F., P. H. Flamant, J. Cuesta, and D. Bruneau (2008), Vertical 2-μ m heterodyne differential absorption lidar measurements of mean CO_2 mixing ratio in the troposphere, *J. Atmos. Oceanic Technol.*, *25*(9), 1477–1497.

Guerlet, S., et al. (2013), Impact of aerosol and thin cirrus on retrieving and validating XCO_2 from GOSAT shortwave infrared measurements, *J. Geophys. Res. Atmos.*, *118*(10), 4887–4905, doi:10.1002/jgrd.50332.

Kuze, A., H. Suto, M. Nakajima, and T. Hamazaki (2009), Thermal and near infrared sensor for carbon observation Fourier-transform spectrometer on the greenhouse gases observing satellite for greenhouse gases monitoring, *Appl. Opt.*, *48*(35), 6716–6733.

Kuze, A., et al. (2011), Vicarious calibration of the GOSAT sensors using the railroad valley desert playa, *IEEE Trans. Geosci. Remote Sens.*, *49*(5), 1781–1795.

Liu, C., et al. (2014), Profile information on co from sciamachy observations using cloud slicing and comparison with model simulations, *Atmos. Chem. Phys.*, *14*(3), 1717–1732.

Mao, J., and S. R. Kawa (2004), Sensitivity studies for space-based measurement of atmospheric total column carbon dioxide by reflected sunlight, *Appl. Opt.*, *43*(4), 914–927.

Menzies, R. T., G. D. Spiers, and J. Jacob (2014), Airborne laser absorption spectrometer measurements of atmospheric co2 column mole fractions: Source and sink detection and environmental impacts on retrievals, *J. Atmos. Oceanic Technol.*, *31*(2), 404–421.

Ramanathan, A., J. Mao, G. R. Allan, H. Riris, C. J. Weaver, W. E. Hasselbrack, E. V. Browell, and J. B. Abshire (2013), Spectroscopic measurements of a CO_2 absorption line in an open vertical path using an airborne lidar, *Appl. Phys. Lett.*, *103*(21), 214102.

Rayner, P., and D. O'Brien (2001), The utility of remotely sensed CO_2 concentration data in surface source inversions, *Geophys. Res. Lett.*, *28*(1), 175–178.

Riris, H., K. Numata, S. Li, S. Wu, A. Ramanathan, M. Dawsey, J. Mao, R. Kawa, and J. B. Abshire (2012), Airborne measurements of atmospheric methane column abundance using a pulsed integrated-path differential absorption lidar, *Appl. Opt.*, *51*(34), 8296–8305.

Rothman, L., et al. (2009), The *HITRAN* 2008 molecular spectroscopic database, *J. Quant. Spectros. Radiat. Transfer*, *110*(9), 533–572.

Sassen, K., and Z. Wang (2008), Classifying clouds around the globe with the CloudSat radar: 1-year of results, *Geophys. Res. Lett.*, *35*, L04805, doi:10.1029/2007GL032591.

Sassen, K., Z. Wang, and D. Liu (2008), Global distribution of cirrus clouds from Cloudsat/Cloud-Aerosol Lidar And Infrared Pathfinder Satellite Observations (CALIPSO) measurements, *J. Geophys. Res.*, *113*, D00A12, doi:10.1029/2008JD009972.

Stephan, C., M. Alpers, B. Millet, G. Ehret, P. Flamant, and C. Deniel (2011), Merlin: A space-based methane monitor, in *SPIE Optical Engineering+ Applications*, pp. 815,908–815,908, International Society for Optics and Photonics, San Diego, Calif.

Stull, R. B. (1988), *An Introduction to Boundary Layer Meteorology*, vol. 13, Springer, Netherlands.

Tiwari, Y. K., M. Gloor, R. J. Engelen, F. Chevallier, C. Rödenbeck, S. Körner, P. Peylin, B. H. Braswell, and M. Heimann (2006), Comparing CO_2 retrieved from atmospheric infrared sounder with model predictions: Implications for constraining surface fluxes and lower-to-upper troposphere transport, *J. Geophys. Res.*, *111*, D17106, doi:10.1029/2005JD006681.

Vay, S. A., et al. (2003), Influence of regional-scale anthropogenic emissions on CO_2 distributions over the western North Pacific, *J. Geophys. Res.*, *108*, 8801, doi:10.1029/2002JD003094.

Ziemke, J., S. Chandra, and P. Bhartia (1998), Two new methods for deriving tropospheric column ozone from toms measurements: Assimilated UARS MLS/HALOE and convective-cloud differential techniques, *J. Geophys. Res.*, *103*, 22,115–22,127.

Ziemke, J., S. Chandra, and P. Bhartia (2001), "Cloud slicing": A new technique to derive upper tropospheric ozone from satellite measurements, *J. Geophys. Res.*, *106*(D9), 9853–9867.

 ©2015. American Geophysical Union. All Rights Reserved.